CHEMIJA. 2013. Vol. 24. No. 3. P. 190–196

Electrochemical study of Mg-Nb alloy films in Hank's solution

Asta Grigucevičienė*,

Laurynas Staišiūnas,

Povilas Miečinskas,

Raimondas Giraitis,

Konstantinas Leinartas,

Eimutis Juzeliūnas

Centre of Physical Sciences and Technology, Institute of Chemistry, A. Goštauto 9, LT-01108 Vilnius, Lithuania

Nanocrystalline Mg-Nb alloy films were sputter-deposited on glass substrates in a wide range of Nb concentrations. XRD studies revealed substitutional solid solutions of Nb in *hcp* Mg lattice when Nb concentrations were up to 26 at.%. At higher Nb concentrations, a *bcc* structure of Nb lattice was determined. An increase in Nb concentration led to contraction of the lattice as well as refining of the alloy, which was evident from reduced crystallographic *c*-parameter along with the grain size. Voltammetric studies in Hank's solution showed that corrosion rate of the alloys decreased with Nb concentration. This was due to reduction of the active electrode area with preferential inhibition of partial anodic reaction. Application of the studied systems as biodegradable materials *in vivo* is discussed.

Key words: Mg-Nb alloy films, Hank's solution, magnetron sputtering

INTRODUCTION

High intrinsic susceptibility to corrosion of magnesium is considered as a drawback when applying this metal (or alloys) in numerous technical fields, such as automotive and aircraft industries, computers and portable electronics. In biomedical applications, however, corrosion activity could be a beneficial property, which makes it possible to dissolve implants *in vivo*. Due to inherent biocompability of Mg and valuable mechanical properties, which are similar to those of human bones, Mg alloys are appreciated for fabrication of biodegradable implants for osteosynthesis, cardiovascular stents or tissue scaffolds [1–29]. This novel class of biomaterials is expected to support a healing process of a tissue and degrade thereafter. This means no need for secondary surgery to remove the implant when only temporary presence of it is necessary.

Magnesium is one of main constituents of human bone and the essential element in a muscle or soft tissue. Mg^{2+} ions are most common in the human body after Na^{+}, Ca^{2+} and K^{+}. These ions stabilize structure of DNA and RNA and are important for several metabolic enzymes [11]. A deficiency in magnesium causes dysfunction of cell membrane and increases incidence of cancer, heart disease and oxidative stress. The toxic dose of magnesium is unknown. Cytotoxic activity of released Mg^{2+} from Mg on osteoblast cells was not

* Corresponding author. E-mail: asta@chi.lt

determined [12]. To the contrary, magnesium in damaged locus supports activity of surrounding bone cells and promotes bone growth [2, 9]. Also, mechanical properties of Mg based alloys are superior to support the human bone when compared to such permanent materials as Ti, stainless steel or Co-Cr alloy [9, 12, 13].

From the viewpoint of biodegradability, Mg alloys are attractive candidates as well. The important requirement is a uniform corrosion at sufficiently low rates especially during initial stages after implantation. For instance, for stents, appreciable degradation start is after some 6 months followed by the vessel reconstruction period completed within next 6 months [7]. The total degradation of the implant during a period of 12 to 24 months is desired [7, 26]. It is important to adjust the degradation rate so that to avoid an intolerable accumulation of the degradation products such as hydrogen or alloying components. There are several ways proposed to control the corrosion behavior of Mg alloys *in vivo*: alloying and tailoring the composition, application of coatings made of more resistant materials such as ceramics, polymer, composite layers [3, 4, 9, 10, 15–26]. Biocompability and toxicity are main issues regarding the modified surfaces and the additives. For instance, widely used alloying elements such as Al, Zn, Mn may cause harmful effects [17, 25, 28–31]. Studies have shown that Al may induce dementia, Mn can cause neurotoxicity leading to Parkinsonism, Zr is closely associated with liver, lung, breast or nasopharyngeal cancer.

Although degradable Mg biomaterials are actively investigated, new effective products are still in great demand. In particular, biocompatible and non-toxic alloying elements are a matter of great relevance. In this study we investigate Nb as a possible candidate. This valve metal readily forms protective surface oxide and, therefore, has excellent corrosion resistance in most aqueous environments. Nb does not dissolve in Mg matrix neither form intermetallic phases with it [32, 33]. Nb is known to be non-toxic and physiologically inert [34, 35]. When treated with sodium hydroxide, Nb forms a bonelike oxide layer that aids osteointegration [34] and prevents corrosion [35].

Little is known about electrochemistry and corrosion behaviour of Mg-Nb alloys, although first report on sputter co-deposition of Mg and Nb was reported about two decades ago [36]. Recently such alloys attracted attention as perspective materials for hydrogen storage devices or switchable mirrors [37]. There is very limited knowledge about electrochemical and corrosion properties of Mg-Nb alloys in biological environments. Our study aims to fill this gap.

EXPERIMENTAL

Magnetron sputtering of Mg and Nb targets was performed using a Univex 350 vacuum system from Leybold Vacuum GmbH (Germany) equipped with two confocal DC magnetrons. Primarily the sputtering chamber was evacuated up to ~2.2×10^{-6} mbar and then filled with working gas (Ar), maintaining a constant pressure at 1.6×10^{-3} mbar. Targets were prepared from high purity Mg (99.9%) and Nb (99.9%) both from Alfa Aesar GmbH (Germany). During deposition the samples (glass discs of 14 mm in diameter were used as substrates) were kept at constant temperature of 60 °C by an integrated infrared heater. The sputtering power used was 95 to 110 W for Mg target and 5 to 90 W for Nb one. The holder of substrates was rotated at a constant velocity of 13 rpm to ensure uniform coating distribution. The ratio of components in Mg-Nb alloys was changed by means of varying sputtering power of both magnetrons. Thickness of as-deposited thin film Mg-*x*Nb alloys was ca. 400–500 nm. After sputtering the samples were kept in a chamber in N_2 atmosphere at ambient conditions for 24 hours.

Composition of Mg-Nb alloys was examined by the microprobe of a scanning electron microscope (SEM) using an EVO-50EP device from Carl Zeiss SMT AG (Germany) equipped with a secondary electron detector. Compositions of the alloys in the paper are given in atomic %, e. g. Mg-4-Nb.

Crystallographic structures of deposited alloys were studied by X-ray diffraction (XRD) using a D8 Advance diffractometer from Bruker AXS (Germany) equipped with the Goebel mirror – a primary beam monochromator for CuKα radiation. A step-scan mode was used in the 2Θ range from 30 to 70° with a step length of 0.02° and a counting time of 5 seconds per step.

Open circuit potential (E_{ocp}) and voltammetric measurements were carried out using a P/G/FRA system PARSTAT 2273 from Princeton Applied Research Instr. (USA). Electrochemical studies were performed in a naturally aerated Hank's Balanced Salt Solution (HBSS) from Sigma Aldrich (Germany). Composition of Hank's solution was (g/l) 0.185 $CaCl_2 \times 2H_20$, 0.097 $MgSO_4$, 0.4 KCl, 0.06 KH_2PO_4, 0.35 $NaHCO_3$, 8.0 NaCl, 0.048 Na_2HPO_4, 1.0 Glucose and 0.011 Phenol Red, pH 7.2–7.6. Phenol Red is used for visual control of HBSS pH. All electrochemical measurements were performed at 20 ± 1 °C. Ag/AgCl (in saturated KCl) was used as a reference electrode and all potential values throughout the paper are referred to this electrode. Platinum plate of ~4 cm^2 area was used as a counter electrode. The working electrode (glass disc with deposited Mg-*x*Nb alloy) was mounted in a special holder and placed into a three-electrode electrochemical glass cell. The area of working electrode surface exposed to electrolyte was 0.5 cm^2. The measured and / or calculated kinetic parameters in the paper are given in respect to the geometrical area of electrode. Tafel polarization curves were measured in the potentiodynamic mode at the potential scan rate 5 mV/s and were used for determination of corrosion current densities (j_{corr}) of studied alloys.

Optical inspection and images of as-prepared and corrosion damaged surfaces were performed by a B-353 Met microscope from Optika Microscopes (Italy), equipped with a digital camera Optikam B 2.0.

RESULTS AND DISCUSSIONS

Crystallographic structure of the sputter-deposited alloys was studied by XRD (Figs. 1 and 2). Figure 1 shows the patterns obtained for Mg-Nb systems with different Nb content (4, 9, 14, 26 and 32 at.%). The pronounced peaks of diffractograms indicate a crystalline structure of the deposits with the prevailing crystallite orientation <001>. The alloys are substitutional solid solutions of Nb in Mg lattice when Nb concentration is up to 26 at.%. This does not hold, however, at higher concentrations (e. g. Mg-32Nb). It is well known that structural parameters of a solid solution depend on those of solute metal. Figure 1 shows that XRD peaks of Mg shift towards higher 2Θ values when Nb concentration is

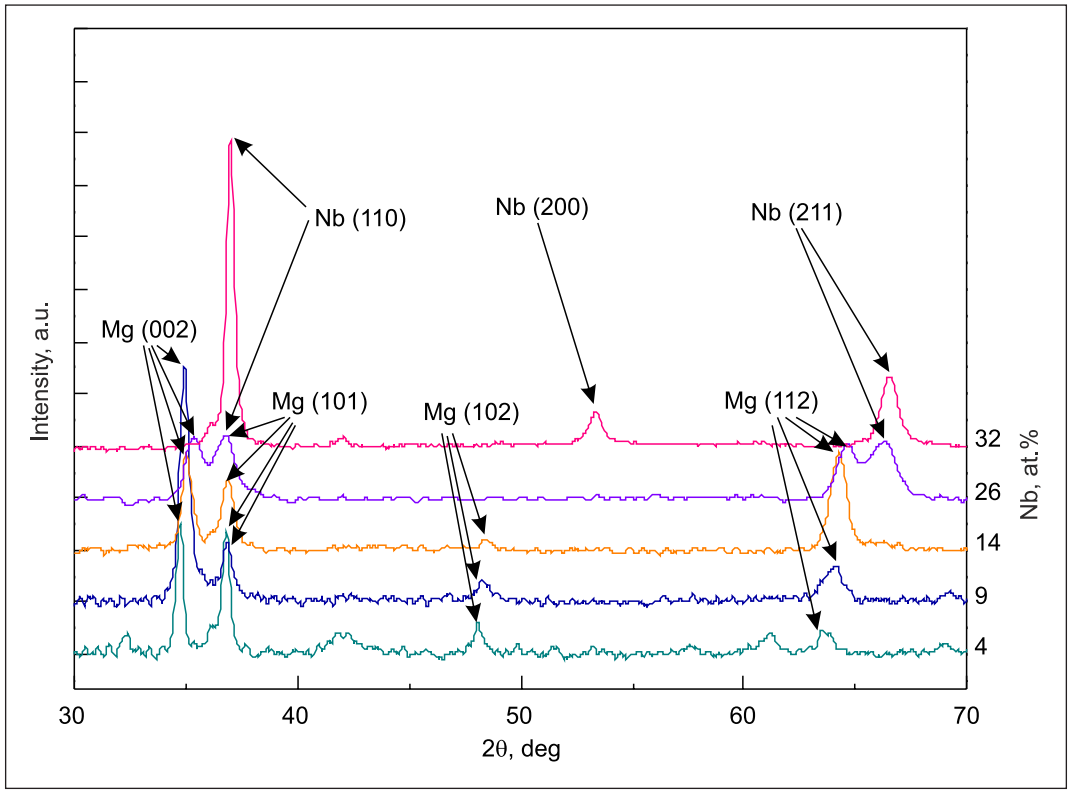

Fig. 1. XRD patterns of magnetron sputtered Mg-xNb alloys. Nb content (*x*) is given in the Figure in atomic %

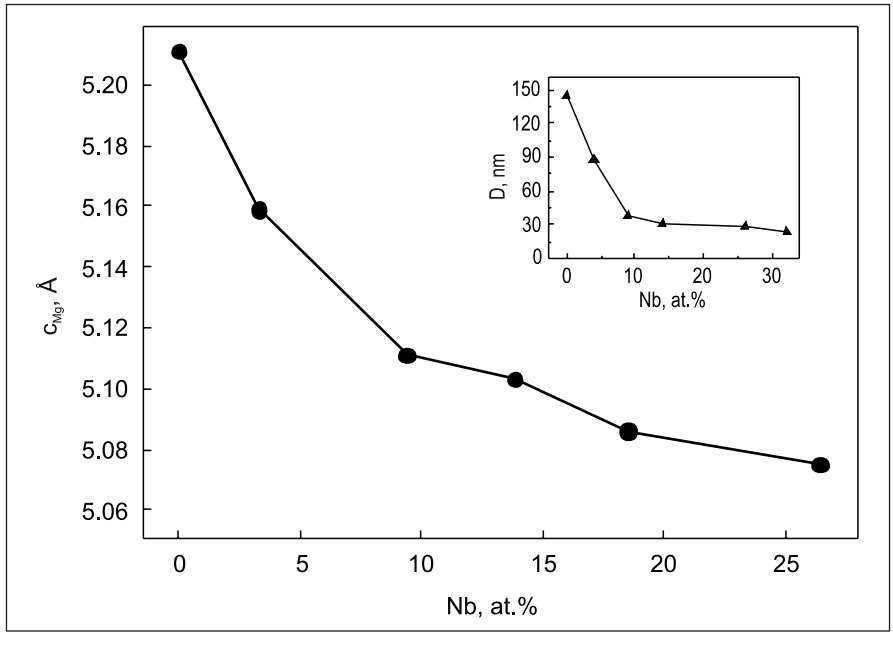

Fig. 2. Dependences of parameter c_{Mg} of Mg *hcp* lattice and average grain sizes of coatings (in insert) on Nb content

increased. The shift is caused by a decrease in lattice parameters of Mg due to the partial substitution of larger Mg atoms by smaller Nb ones. The atomic radii of these atoms are 0.15985 and 0.14318 nm, respectively [38]. A hexagonal closed packed (*hcp*) structure is characteristic of Mg and it is also retained for the alloys with the concentration up to ~26 at.% of Nb (Fig. 1). The lattice parameter c_{Mg} of the *hcp* structure decreases with increase in Nb concentration (Fig. 2). According to the Vegard's law, the crystal lattice parameter of alloy linearly depends on the concentration of constituent elements. However, some deviation from linearity is true for the system studied. It is obvious that the contraction of Mg lattice implies superior strength and hardness of Mg-Nb alloys when compared to those of pure magnesium. Introduction of Nb atoms into Mg lattice also induces grain-refinement effect. Average grain sizes of coatings were evaluated from XRD data according to the Scherrer's formula:

$$D = 0.94\lambda/\beta \cos\Theta, \quad (1)$$

where D is the grain size in nanometers, λ is the X-ray wavelength (λ = 0.154062 nm for CuK_α radiation) and Θ is the diffraction angle of the peak. The β stands for the width of the pure diffraction profile on the 2Θ scale in radians, which has been obtained according to

$$\beta = B - b, \quad (2)$$

where B is the integral width at a half of the maximum intensity for a sample, and b is that for a standard (LaB_6, for which b = 0.016 rad was used). The β value was calculated according to the width of the Mg 002 peak. It was found that the alloys are nanocrystalline ones with the grain sizes (D) of the order of several tens of nanometers (Fig. 2). The grain size clearly decreases with increase in Nb content. It is noteworthy that shapes of both *c*- and *D*-curves are similar. The refinement is important from the viewpoint of corrosion resistance of metals. Fine-grained sputtered alloys usually exhibit higher passivity than the cast counterparts, as it was demonstrated, for instance, for sputtered Mg-Al alloys [39].

It is important that at higher Nb concentrations the alloys show the presence of cubic body centred (*bcc*) structure (e. g. 26 and 32 at.%, curves 4 and 5 in Fig. 1). Only minor quantity of the *bcc* phase was found for Mg-26Nb alloy, whereas for Mg-32Nb alloy the *bcc* phase of Nb was prevailing. Probably, a transition from the *hcp* structure to *bcc* is the reason why the *c*-curve in Fig. 2 is not linear, at low Nb concentrations alloy has a prevailing *hcp*-phase and at high concentrations alloy has a prevailing *bcc* structure. The most probable cause of deviation from linearity is that formation of Nb *bcc* lattice in coating led to lesser quantity of Nb in Mg *hcp* lattice.

Open circuit potential (E_{ocp}) provides information on electrochemical (corrosion) stability of the alloys. The curves E_{ocp} vs. exposure time are given in Fig. 3. The initial E_{ocp} values are within the ranges ~–1.4 to ~–1.2 $V_{Ag/AgCl}$. A positive potential shift is observed during the exposure, which means an increase in electrode passivity. A quasi-steady-state value is attained after some 10–20 min of exposure. These values do not differ greatly for the alloys with 4 to 26 at.% of Nb. Substantial ennoblement exhibits alloy

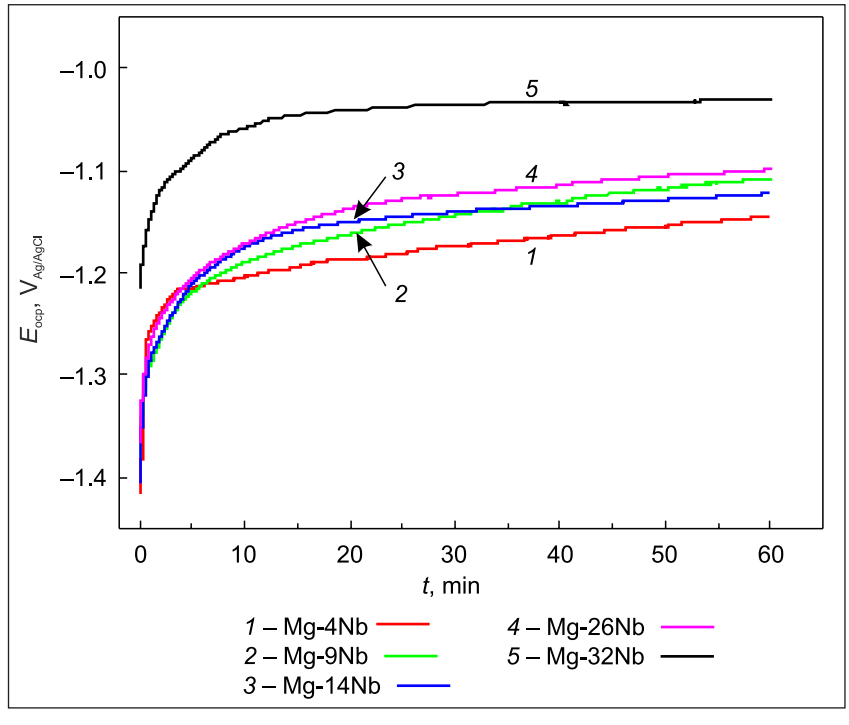

Fig. 3. Dependence of E_{ocp} of magnetron-sputtered Mg-xNb alloys in Hank's solution on Nb content in alloy

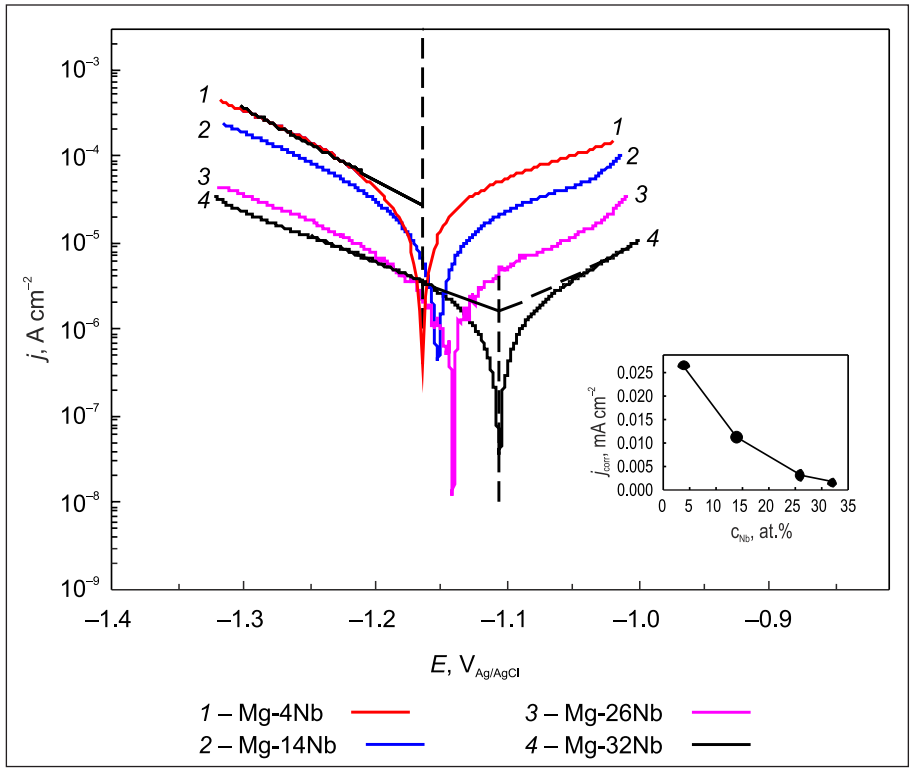

Fig. 4. Tafel dependences of magnetron-sputtered Mg-xNb alloys in Hank's solution. Insert: dependence of j_{corr} on Nb content. An extrapolation from Tafel regions to E_{corr} is shown for Mg-4Nb and Mg-32Nb alloys

Table. j_{corr} and respective corrosion rates of Mg-xNb alloys

Alloy	Mg-4Nb	Mg-14Nb	Mg-26Nb	Mg-32Nb
j_{corr}, mA/cm^2	2.68×10^{-5}	1.12×10^{-5}	3.0×10^{-6}	1.6×10^{-6}
Corrosion rate, mm/year	0.61	0.25	0.068	0.036

with 32 at.% of the additive. The most probable reason of such ennoblement is an enrichment of the alloy surface by Nb oxide, which has much higher protective capability when compared to Mg oxide.

Electrochemical behaviour of the systems in Hank's solution was studied by dc-voltammetry (Fig. 4). Anodic and cathodic curves (Tafel plots) were recorded after a quasi-steady-state has been attained (Fig. 3). Obviously, when increasing Nb concentration, the *E-j* plots shift down and open circuit potential increases. The slope of cathodic Tafel plots is observed about 120–140 mV, which implies cathodic hydrogen evolution with a charge transfer control. On the contrary, anodic slopes change significantly when Nb concentration is increased: from ~200 mV for Mg-4Nb to ~130 mV for Mg-32Nb (curves 1 and 4). The last value is in line with the Mg corrosion mechanism according to which formation of the intermediate Mg^+ ions is the first step of dissolution [40, 41]. At the same time, considerably higher values of measured anodic slopes for alloys with low Nb concentration are due to the Negative Difference Effect, i. e. the increase of hydrogen evolution rate with the increase of anodic potential. It can be concluded that Nb acts as an inhibitor, which reduces the active surface area without changing remarkably the corrosion mechanism, i. e. electrochemical reactions of water decomposition and Mg dissolution. The positive E_{ocp} shift implies that the inhibiting influence is more pronounced in respect to the anodic process.

As commonly known, extrapolation of Tafel plots to E_{ocp} (or corrosion potential) gives the corrosion current density (j_{corr}). Such data are provided in the insertion in Fig. 4. It can be seen that introduction of 32 at.% of Nb leads to reduction of corrosion activity of about one order of magnitude. The j_{corr} values (mA cm^{-2}) may be converted to mm per year (mm/year). Such data are given in Table. These corrosion rates are only a rough approximation as they assume corrosion process to be uniform. For exact evaluation of Mg corrosion rate the method of Tafel extrapolation must be complemented by other ones: weight loss and hydrogen evolution.

Figure 5 shows optical views of the surfaces. As-deposited samples are compared with those exposed in Hank's solution. Obviously, at lower Nb concentrations, the surface is severely affected by corrosion. At higher Nb concentration, substantial mitigation of the corrosion attack is evident. In this case, there are no continuously corroded areas; just some localized corrosion sites are visible (Fig. 5e, f).

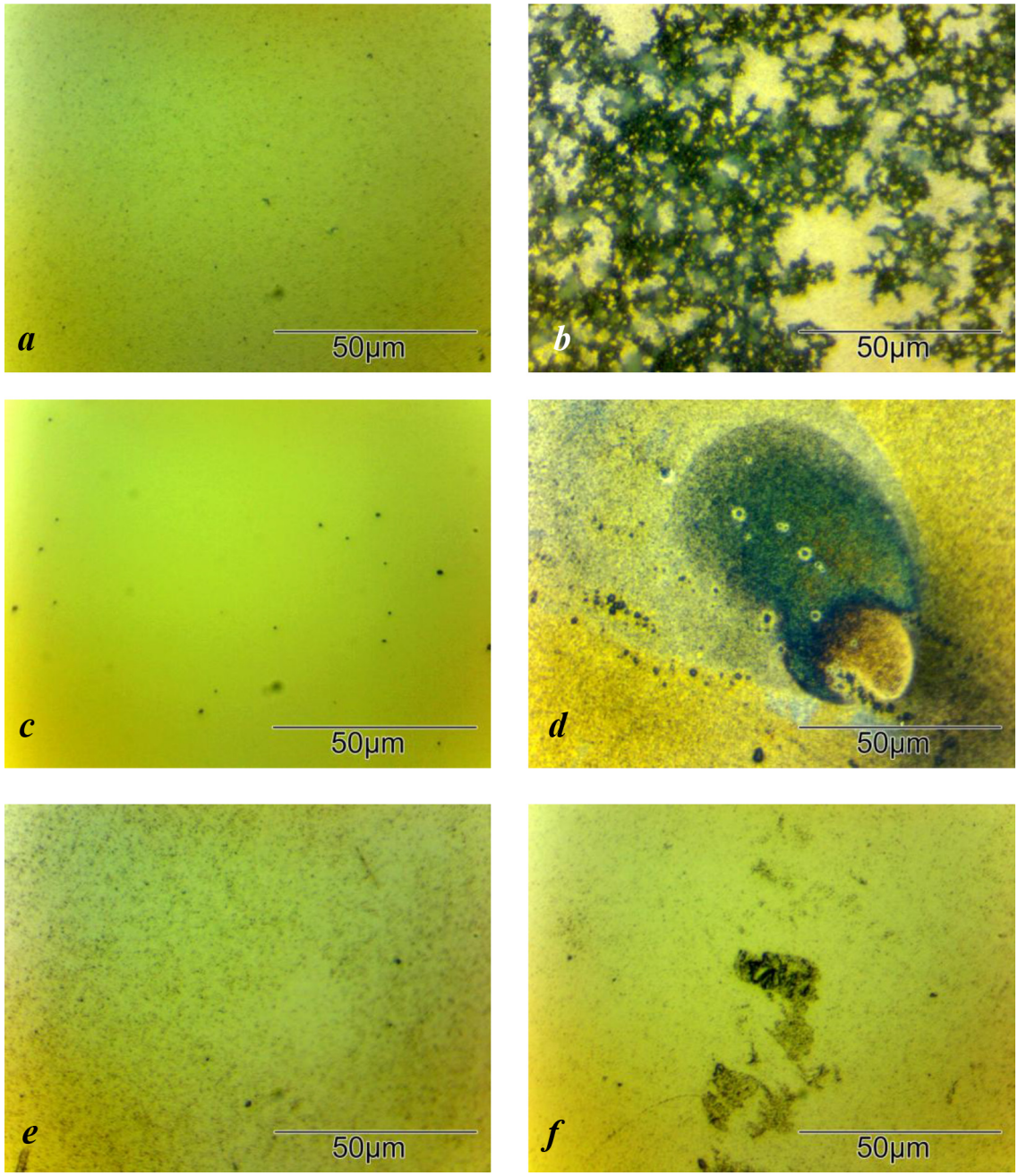

Fig. 5. Optical images of surfaces of Mg-4Nb (*a*, *b*), Mg-14Nb (*c*, *d*) and Mg-32Nb (*e*, *f*) alloys: as-prepared (*a*, *c*, *e*) and after 10 min exposure in Hank's solution (*b*, *d*, *f*)

CONCLUSIONS

1. Mg-*x*Nb alloys with Nb content ranging between 4 and 32 at. % were formed by magnetron sputtering. The alloys had crystalline structures with grain sizes of the order of several tens of nanometers.

2. Increase in Nb content leads to higher corrosion resistance of the alloys in Hank's solution. Corrosion rates of Mg alloy decreased almost tenfold when the concentration of Nb was increased from 4 to 32 at.%.

3. Corrosion process of Mg-Nb alloys could be tailored to *in vivo* needs by proper selection of Nb concentration.

ACKNOWLEDGEMENTS

The study has been supported by the Research Council of Lithuania (Contract MIP-119/2012).

Received 22 May 2013
Accepted 18 June 2013

References

1. B. Heublein, R. Rohde, V. Kaese, M. Niemeyer, W. Hartung, A. Haverich, *Heart*, **89**, 651 (2003).

2. F. Witte, V. Kaese, H. Haferkamp, et al. *Biomaterials*, **26**, 3557 (2005).
3. M. P. Staiger, A. M. Pietak, J. Huadmai, G. Dias, *Biomaterials*, **27**, 1728 (2006).
4. F. Witte, *Acta Biomater.*, **6**, 1680 (2010).
5. M. Alvarez-Lopez, M. D. Pereda, J. A. del Valle, et al., *Acta Biomater.*, **6**, 1763 (2010).
6. N. T. Kirkland, J. Lespagnol, N. Birbilis, M. P. Staiger, *Corros. Sci*., **52**, 287 (2010).
7. H. Hermawan, D. Dubé, D. Mantovani, *Acta Biomater.*, **6**, 1693 (2010).
8. N. Hort, Y. Huang, D. Fechner, et al., *Acta Biomater.*, **6**, 1714 (2010).
9. A. Purnama, H. Hermawan, J. Couet, D. Mantovani, *Acta Biomater*., **6**, 1800 (2010).
10. H. Hornberger, S. Virtanen, A. R. Boccaccini, *Acta Biomater.*, **8**, 2442 (2012).
11. A. Hartwig, *Mutat. Res.*, **475**, 113 (2001).
12. Y. H. Yun, Z. Dong, D. Yang, et al., *Mat. Sci. Eng. C*, **29**, 1814 (2009).
13. L. Kouisni, M. Azzi, M. Zertoubi, F. Dalard, S. Maximovitch, *Surf. Coat. Tech*., **185**, 58 (2004).
14. M. M. El-Omar, G. Dangas, I. Iakovou, R. Mehran, *Curr. Interv. Cardiol. Rep.,* **3**, 296 (2001).
15. V. T. Kaesel, P. T. Tai, F. W. Bach, H. Haferkamp, F. Witte, H. Windhagen, *Proceedings of the Sixth International Conference: Magnesium Alloys and their Applications*, Wiley VCH, New York (2004).
16. N. Hort, Y. Huang, D. Fechner, et al., *Acta Biomater*., **6**, 1714 (2010).
17. G. Song, *Corr. Sci.*, **49**, 1696 (2007).
18. N. C. Quach, P. J. Uggowitzer, P. Schmutz, *C. R. Chim.,* **11**, 1043 (2008).
19. A. C. Hanzi, P. Gunde, M. Schinhammer, P. J. Uggowitzer, *Acta Biomater.*, **5**, 162 (2009).
20. M. Liu, P. Schmutz, P. J. Uggowitzer, G. Song, A. Atrens, *Corr. Sci.*, **52**, 3687 (2010).
21. A. C. Hanzi, I. Gerber, M. Schinhammer, J. F. Löffler, P. J. Uggowitzer, *Acta Biomater.*, **6**, 1824 (2010).
22. P. Gunde, A. C. Hänza, A. S. Sologubenko, P. J. Uggowitzer, *Mater. Sci. Eng. A*, **528**, 1047 (2011).
23. T. Kraus, S. F. Fischerauer, A. C. Hanzi, P. J. Uggowitzer, J. F. Löffler, A. M. Weinberg, *Acta Biomater.*, **8**, 1230 (2012).
24. H. Wang, Y. Estrin, Z. Zuberova, *Mater. Lett*., **62**, 2476 (2008).
25. L. Li, J. Gao, Y. Wang, *Surf. Coat. Technol*., **185**, 92 (2004).
26. Y. Wang, M. Wei, J. Gao, *Mater. Sci. Eng. C*, **29(4)**, 1311 (2009).
27. Y. Song, S. Zhang, J. Li, C. Zhao, X. Zhang, *Acta Biomater.*, **6**, 1736 (2010).
28. C. K. Yuen, W. Y. Ip, *Acta Biomater.*, **6**, 1808 (2010).
29. Z. Li, X. Gu, S. Lou, Y. Zheng, *Biomater.*, **29**, 1329 (2008).
30. T. D. Lucey, B. Venugopal, *Metal Toxicity in Mammals*, Plenum Press, NJ (1977).
31. J. Crossgrove, W. Zheng, *NMR Biomed.*, **17**, 544 (2004).
32. A. A. Nayeb-Hashemi, J. B. Clark, *Phase Diagrams of Binary Magnesium Alloys*, ASM International, Materials Park, OH 44073 (1988).
33. H. K. Westengen, in: K. H. Jurgen, R. W. Cahn, M. C. Flemings, B. Ilschner, E. J. Kramer, S. Mahajan (eds.), *Encyclopedia of Materials: Science and Technology*, Elsevier Science Ltd. (2001).
34. R. Godley, D. Starosvetsky, I. Gotman, *J. Mater. Sci.-Mater. M.*, **15(10)**, 1073 (2004).
35. V. V. Starikov, S. L. Starikova, A. G. Mamalis, S. N. Lavrynenko, J. J. Ramsden, *J. Bio. Phys. Chem*., **7(4)**, 141 (2007).
36. E. Hirota, H. Habazaki, A. Kawashima, K. Asami, K. Hashimoto, *Sci. Rep. Res. Tohoku*, **A38**, 53 (1993).
37. S. Bao, K. Tajima, Y. Yamada, P. Jin, M. Okada, K. Yoshimura, *Jpn. J. Cer. Soc*., **116(6)**, 771 (2008).
38. *XRD database "Powder Diffraction File-2" (integrated part of D8 Advance Diffractometer software).*
39. A. Griguceviciene, K. Leinartas, R. Juskenas, E. Juzeliunas, *J. Electroanal. Chem.*, **565**, 203 (2004).
40. G. Song, A. Atrens, *Adv. Eng. Mat*., **5**, 837 (2003).
41. Z. Shi, M. Liu, A. Atrens, *Corr. Sci.*, **52**, 579 (2010).

Asta Grigucevičienė, Laurynas Staišiūnas, Povilas Miečinskas, Raimondas Giraitis, Konstantinas Leinartas, Eimutis Juzeliūnas

Mg-Nb LYDINIO ELEKTROCHEMINIAI TYRIMAI HANK'O TIRPALE

S a n t r a u k a

Plonos nanokristalinių Mg-Nb lydinių dangos buvo formuojamos ant stiklo substratų pastoviosios srovės magnetroninio dulkinimo metodu. Rentgeno spindulių difrakcijos metodu nustatyta, kad lydiniai, kuriuose Nb koncentracija yra iki 26 at.%, suformuoja Nb pakaitinius kietus tirpalus Mg heksagoninėje tankioje gardelėje. Esant didesnei Nb koncentracijai formuojasi Nb centruoto tūrio kubinė gardelė. Nb koncentracijos didėjimas Mg gardelėje lemia jos susitraukimą (nustatyta pagal kristalografinio c parametro mažėjimą) ir dangos kristalitų dydžio mažėjimą. Voltamperometriniais matavimais Hank'o tirpale nustatyta, kad didėjant Nb koncentracijai lydinyje mažėja jų korozijos greitis. Tai sietina su elektrodo aktyvaus ploto sumažėjimu ir preferenciniu anodinės reakcijos lėtinimu. Aptarta galimybė panaudoti tirtus lydinius kaip biodegraduojančias medžiagas.